ISSN: 2414-1895 DOI: 10.6919/ICJE.202312_9(12).0068

Finite Element Analysis and Verification of Variable Geometry Aircraft Flexible Structures

Yuhang Zou[a], Yabo Yu[b], Boyu Jiang[c]

Northeastern University, School of Metallurgy, Shenyang 110819, China

[a]2745457260@qq.com, [b]674934010@qq.com, [c]1692540237@qq.com

Abstract

In recent years, the rapid advancement of the aerospace industry has underscored the increasing importance of research on variable geometry aircraft. Firstly, this paper presented the current state of domestic and international research on the relevant structures of variable geometry aircraft. Subsequently, two flexible structures were analyzed and compared by finite element software. One was subjected to torsional loading to observe its deformation in three-dimensional space, while the other was subjected to tensile loading to observe its deformation in two-dimensional space. To ensure the accuracy of the finite element analysis results, various comparative methods were employed for validation. This study provides a reference and foundation for related research in the field of variable geometry aircraft.

Keywords

Variable Geometry Aircraft; Flexible Structures; Finite Element Analysis; ANSYS; Comparative Verification.

1. Introduction

The concept of variable geometry, which can be traced back to as early as 1916, has gained increasing attention in the field of aerospace as technology continues to advance rapidly. Variable geometry aircraft is considered the future of aviation development and has become a subject of great interest among scholars both domestically and internationally, with a focus on various key topics within the domain of variable geometry aircraft structures [1-4].

Perry I initiated the Active Flexible Wing (AFW) project to explore the application of flexible wings in high-performance fighter aircraft. This project aimed to reduce structural weight, prevent control surface flutter, and enhance control capabilities [5]. Garcia and his team designed a wing with the ability to twist for micro air vehicles, with a specific focus on studying its roll control capabilities. Simulation results demonstrated that wing twist deformation could significantly improve the roll rate and, consequently, enhance the roll control of the aircraft. To further verify the concept of improving control capabilities through wing twist deformation, Kudva JN and colleagues divided the trailing edge control surface of the wing into ten separate sections, each of which could be individually manipulated using eccentric levers, thus achieving twist deformation of the wing's trailing edge through controlling its curvature [7-10].

Extensive experimental work was complemented by numerical simulations and simulation analysis. Ge Wenjie and his team utilized topology optimization techniques to design a flexible trailing-edge wing and empirically demonstrated the feasibility of flexible wing structures. They also analyzed the influence of geometric parameters on the lift-to-drag characteristics of the wing [11-15].

In conclusion, variable geometry aircraft have been the subject of extensive and in-depth research worldwide. However, the study of fundamental components of variable geometry aircraft remains

ISSN: 2414-1895 DOI: 10.6919/ICJE.202312_9(12).0068

relatively limited. This paper focuses on the flexible and elastic structures of variable geometry aircraft, conducting finite element analysis and analytical validation. The findings presented in this study offer valuable references and foundations for further research in this particular domain.

2. Numerical Calculation

2.1 Geometric Model

Model parameters: Outer diameter D=48.6mm, inner diameter d=44.6mm, hollow network structure vertical rod length L1=10.35mm, diagonal rod length L2=20.7mm. Its physical structure is shown in Fig. 1, and CATIA software is used for modeling, as shown in Fig. 2.

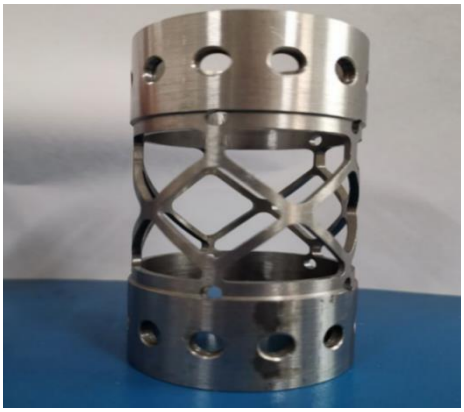

Fig. 1 Tubular flexible and elastic structure

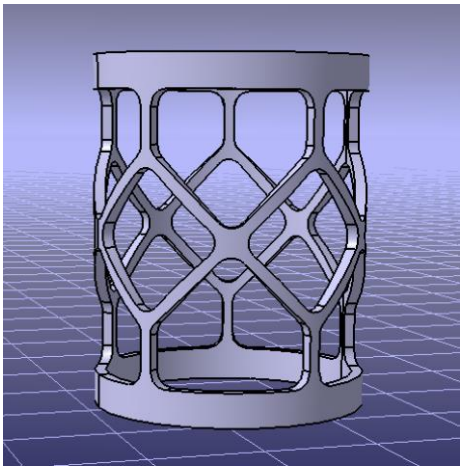

Fig. 2 Three-dimensional model of tubular flexible and elastic structure

To import the three-dimensional model into ANSYS, the first step involves configuring the element properties. The Solid Brick 8 node 185 element type was chosen for this analysis. Subsequently, material properties were defined with an elastic modulus of 200,000 Pa and a Poisson's ratio of 0.3.

2.2 Mesh Generation

ANSYS offers a variety of efficient methods for mesh generation, including free meshing, mapped meshing, extruded meshing, and adaptive meshing. In this study, the free meshing method was employed. Initially, in the Meshing tool dialog box, under the Element Attributes section, Volumes were selected. All entities of the structure were picked, and Element Type 1 and Material 1 were assigned to the entities. The mesh size was set to 1.5, as illustrated in Fig. 3.

ISSN: 2414-1895 DOI: 10.6919/ICJE.202312_9(12).0068

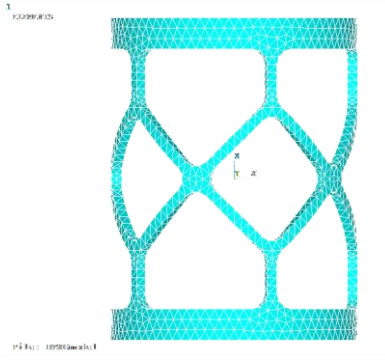

Fig. 3 Mesh Generation

2.3 Application of Loads

To apply the torsional load, a method involving the application of ten opposing tangential forces at the upper and lower circular rings was employed. Clockwise tangential forces were applied at the upper ring, while counterclockwise tangential forces were applied at the lower ring. Each of these applied loads had a magnitude of 3 KN.The upper and lower force points are denoted as A1, B1, C1, D1, E1 and A2, B2, C2, D2 and E2 respectively. As shown in Fig. 4.

2.4 Solution Analysis

2.4.1 Comparative Analysis under Different Loads

The results after finite element solution and analysis are shown in Fig. 5.

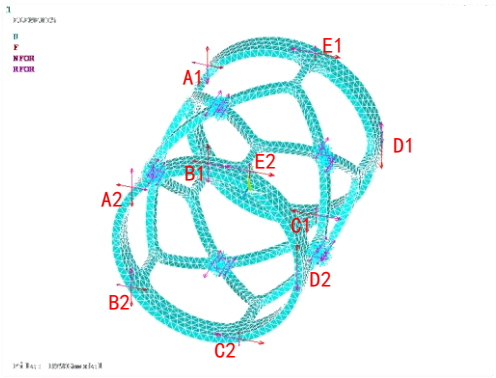

Fig. 4 Position of load application

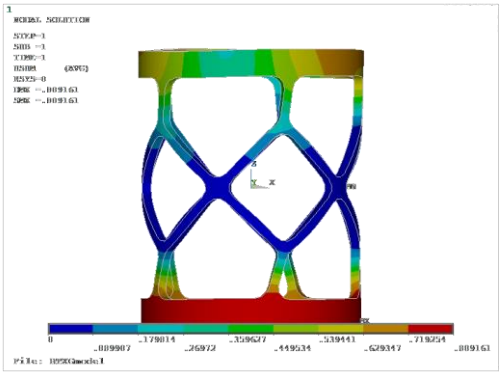

Fig. 5 Cloud map of displacement and deformation
(The load is 3KN)

ISSN: 2414-1895 DOI: 10.6919/ICJE.202312_9(12).0068

Based on the model dimensions and the relationship between displacement and torsional angle, the angles of rotation at various loading points were calculated. The deformation data for the upper circular ring is presented in Table 1, while the data for the lower circular ring is provided in Table 2.

Table 1. Deformation data for the upper circular ring

Load position	**A1**	**B1**	**C1**	**D1**	**E1**	**Mean value**
Load /KN	3	3	3	3	3	3
Displacement /mm	0.67932	0.62084	0.63969	0.57821	0.53688	0.610988
Angle/degree	1.6017	1.4638	1.5083	1.3633	1.2659	1.44168

Table 2. Deformation data for the lower circular ring

Load position	**A2**	**B2**	**C2**	**D2**	**E2**	**Mean value**
Load /KN	3	3	3	3	3	3
Displacement /mm	0.80338	0.77511	0.76853	0.77056	0.79081	0.781678
Angle/degree	1.8943	1.8276	1.8121	1.8169	1.8646	1.8431

The load size is increased from 3KN to 10KN, other conditions remain unchanged, and the analysis results are shown in Fig 6.

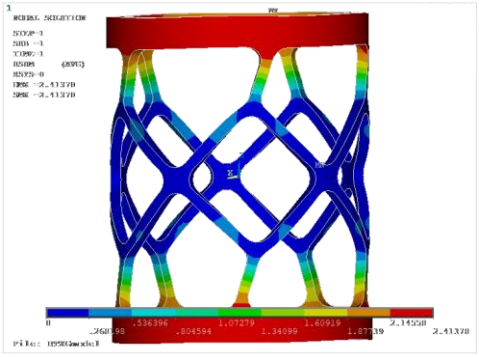

Fig. 6 Displacement and deformation cloud map
(The load is 10KN)

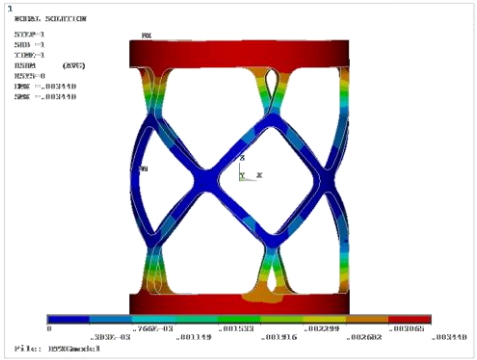

Fig. 7 Displacement and deformation cloud map
(The first loading method)

ISSN: 2414-1895 DOI: 10.6919/ICJE.202312_9(12).0068

The calculation of angular displacement data, based on model dimensions and displacement information, has been carried out. The angular displacement data for the upper circular ring is presented in Table 3, while the data for the lower circular ring is provided in Table 4.

Table 3. Angular displacement data for the upper circular ring

Load position	**A1**	**B1**	**C1**	**D1**	**E1**	**Mean value**
Load /KN	10	10	10	10	10	10
Displacement /mm	2.1791	2.2873	2.3973	2.3930	2.2799	2.30732
Angle/degree	5.1380	5.3932	5.6532	5.6424	5.3756	5.44048

Table 4. Angular displacement data for the lower circular ring

Load position	**A2**	**B2**	**C2**	**D2**	**E2**	**Mean value**
Load /KN	10	10	10	10	10	10
Displacement /mm	2.1221	2.2379	2.3276	2.3047	2.1961	2.23768
Angle/degree	5.0036	5.2766	5.4882	5.4342	5.1780	5.27612

2.4.2 Comparative Analysis under Different Elastic Modulus (The first loading condition)

The elastic modulus of the model was adjusted to 210 GPa while keeping other conditions constant. The analysis results are illustrated in Fig. 7.

The angular displacement data, computed based on the displacement, is presented for the upper circular ring in Table 5 and for the lower circular ring in Table 6.

Table 5. Deformation data for the upper circular ring

Load position	**A1**	**B1**	**C1**	**D1**	**E1**	**Mean value**
Load /KN	10	10	10	10	10	10
Displacement /mm	3.1130	3.2676	3.4248	3.4186	3.2570	3.2962
Angle/degree	7.3400	7.7046	8.0752	8.0606	7.6769	7.77146

Table 6. Deformation data for the lower circular ring

Load position	**A2**	**B2**	**C2**	**D2**	**E2**	**Mean value**
Load /KN	10	10	10	10	10	10
Displacement /mm	3.0316	3.1971	3.3252	3.2963	3.1373	3.1975
Angle/degree	7.1480	7.5382	7.8404	7.7722	7.3972	7.5392

3. Finite Element Analysis with Different Constraints

To validate the accuracy of the previous finite element analysis results, another finite element analysis was conducted under unchanged conditions, utilizing an alternative loading and constraint approach.

3.1 Second Loading Method and Constraint

For the lower circular ring of the model, constraints were introduced, and a torque was applied on the central symmetry plane for analysis. In this analysis, five tangential forces of 1 KN each were applied on the symmetry plane instead of a torque, as illustrated in Fig. 8.

ISSN: 2414-1895 DOI: 10.6919/ICJE.202312_9(12).0068

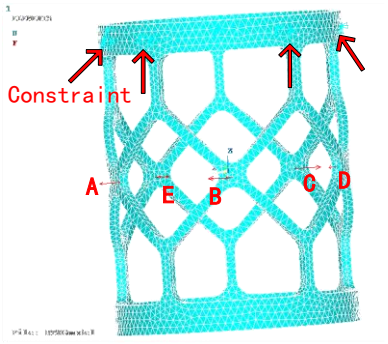

Fig. 8 Load position and constraint position
(The second loading method)

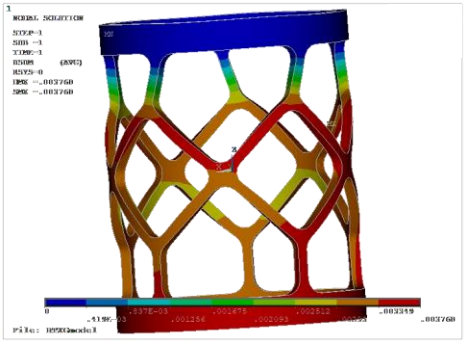

Fig. 9 Displacement and deformation cloud map
(The second loading method)

Table 7. Deformation data for the circular ring

Load position	A	B	C	D	E	Mean value
Load /KN	10	10	10	10	10	10
Displacement /mm	3.3045	3.3124	3.3215	3.2427	3.3381	3.30384
Angle/degree	7.7915	7.8101	7.8316	7.6458	7.8707	7.78994

3.2 Third Loading Method and Constraint

Both ends of the model's circular rings were entirely constrained, and a torque was applied on the central symmetry plane. Instead of a torque, five tangential forces of 10 KN each were applied on the symmetry plane, as depicted in Fig 10. The finite element analysis results are presented in Fig. 11. After calculation, the rotation Angle of each extension point is shown in Table 8.

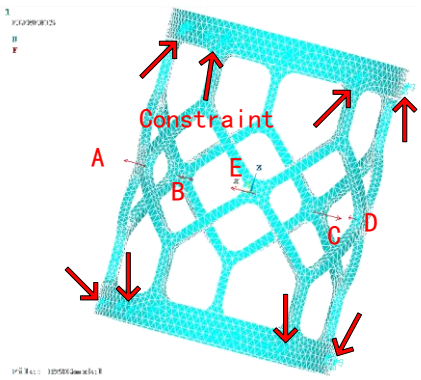

Fig. 10 Load position and constraint position
(The third loading method)

ISSN: 2414-1895 DOI: 10.6919/ICJE.202312_9(12).0068

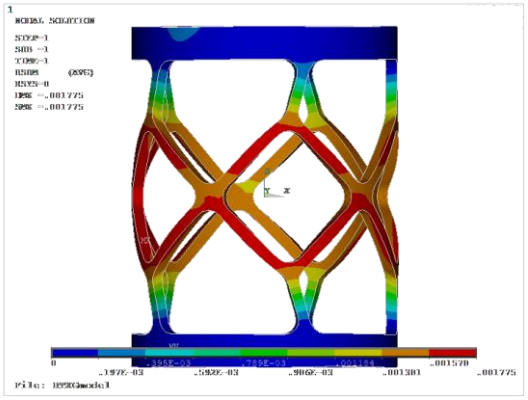

Fig. 11 Displacement and deformation cloud map
(The third loading method)

Table 8. Deformation data for the circular ring

Load position	**A**	**B**	**C**	**D**	**E**	**Mean value**
Load /KN	10	10	10	10	10	10
Displacement /mm	1.6862	1.6096	1.6252	1.5718	1.5849	1.61554
Angle/degree	3.9758	3.7952	3.8320	3.7060	3.7316	3.80812

From the displacement contour plots, it can be observed that the maximum deformations for loading methods 1 and 2 are 3.448 mm and 3.768 mm, respectively, which are nearly identical. In contrast, the maximum deformation for method three is 1.775 mm, approximately half of the values obtained from the first two methods. This discrepancy arises from the fact that the third method applies constraints on both sides of the loading points, whereas the first two methods constrain only one side of the loading points. Consequently, there is a twofold numerical relationship between them, validating the displacement results obtained from the finite element analysis.

The average torsional displacement of the upper circular ring can be calculated from the angles at five loading points (A1 to E1).

$$\bar{\phi}_{up} = \frac{1}{5}\sum_{i=1}^{5}\phi_i = 7.77146°$$

Similarly, the average torsional displacement of the lower circular ring can be determined from the angles at the five loading points (A2 to E2).

$$\bar{\phi}_{down} = \frac{1}{5}\sum_{j=1}^{5}\phi_j = 7.5392°$$

The relative torsional angle $\bar{\phi}_1$ between the upper and lower rings in the first loading method is 15.31066 degrees.

In the second loading method, the average torsional angle on the symmetrical plane is:

$$\bar{\phi}_2 = \frac{1}{5}\sum_{k=1}^{5}\phi_k = 7.78994°$$

ISSN: 2414-1895 DOI: 10.6919/ICJE.202312_9(12).0068

In the third loading method, the average torsional angle is:

$$\bar{\phi}_3 = \frac{1}{5}\sum_{m=1}^{5}\phi_m = 3.80812°$$

Therefore, the relative torsional angles for the upper and lower circular rings in loading method 1 are approximately the same. The average torsional angle on the symmetry plane for loading method 2 is also nearly identical to the average torsional angle for loading method 1, while the average torsional angle for loading method 3 is half that of the other methods.

From the data on torsional angles, it can be observed that the torsional angles for the upper and lower circular rings in loading method 1 and the torsional angles on the symmetry plane for loading method 2 are almost identical, while the torsional angles for loading method 3 are half of the other methods.

By examining the relationships between displacement and angular changes in the figures, it becomes apparent that the deformations for loading methods 1 and 3 are nearly identical, while the deformation for loading method 2 is half that of the other two methods.

Regarding the loading points, loading methods 1 and 3 are both equivalent to applying constraints on one side only, resulting in minimal differences in displacement and angular change. loading method 2, on the other hand, applies constraints on both sides of the loading points, leading to displacement and angular changes that are half of the other two methods.

Through the finite element analysis and comparison of the three methods applied to the model, it is evident that our analysis results should be reasonably accurate and reliable.

4. Analytical Analysis for Comparative Verification

To verify the correctness of the finite element modeling, analytical analysis was conducted on the tubular flexible structure model.

Analytical modeling analysis employed two different constraint modes for examination. The first involved constraining the central symmetry plane and applying torsion to both the upper and lower circular rings. The second method included constraining one of the circular rings and applying torsion at the central symmetry plane.

This analytical process is entirely identical to the first two finite element analysis methods. The analytical modeling analysis data, conducted with an elastic modulus of 210 GPa and a load of 10 KN, is presented in Table 9.

Table 9. Analytical Modeling Analysis Data for Two Methods

	Load/KN	**Displacement**/mm	**Angle**/degree
Loading method 1	10	3.1451	7.6875
Loading method 2	10	3.2043	7.8305

The results of finite element analysis are compared with the data of analytical analysis.

Loading method 1: the displacement and angle of analytical analysis are 3.1451mm and 7.6875 degrees, respectively. In the finite element analysis, the displacement of the two rings is 3.2962mm, 3.1975mm, and the angle is 7.77146 degrees and 7.5392 degrees, respectively.

Loading method 2: the displacement and angle of analytical analysis are 3.2043mm and 7.8305 degrees, respectively. The displacement and angle in finite element analysis are 3.30384mm and 7.78994 degrees, respectively.

(1) Comparison between the analytical derivation of loading method 1 and the simulation results

ISSN: 2414-1895 DOI: 10.6919/ICJE.202312_9(12).0068

Loading method 1 involves unfolding the flexible pipe into a two-dimensional structural model. It simplifies the structure into a "Y"-shaped configuration, taking into account symmetry, and applies a shear force "P" at one end of the "Y" structure with fixed-end constraints at points A and B. Using this simplified model, simulation was conducted using ANSYS software to obtain the relative displacement and torsional angles between the upper and lower steel rings at both ends of the flexible pipe. The comparison for the upper circular ring is presented in Table 10 below:

Table 10. Comparison of analytical derivation and finite element analysis results for the upper circular ring in loading method 1

Relative quantity	Analytic derived value	Finite element analysis value	rror
Relative displacement/mm	3.4104	3.2962	3.35%
Torsion Angle/°	8.0875	7.7715	3.91%

Table 11. Comparison of analytical derivation and finite element analysis results for the lower circular ring in loading method 1

Relative quantity	Analytic derived value	Finite element analysis value	Error
Relative displacement/mm	3.0693	3.1975	4.18%
Torsion Angle/°	7.2788	7.5392	3.585

(2) Comparison between the analytical derivation of loading method 2 and the simulation results

For loading method 2, the flexible pipe was unfolded into a two-dimensional structural model. It was simplified into a "pentagon" shape, leveraging symmetry, with a shear force "P" applied at point O on one end of the "pentagon" structure, and fixed-end constraints at points A and B. Using this simplified model, simulation was conducted using the ANSYS software to obtain the relative displacement and torsional angle between the steel rings at both ends of the flexible pipe. The comparison is illustrated in Table 12 below:

Table 12. Comparison of analytical derivation and finite element analysis results for method 2

Relative quantity	Analytic derived value	Finite element analysis value	Deviation contrast
Relative displacement/mm	3.2043	3.3038	3.11%
Torsion Angle/°	7.6048	7.7899	2.43%

The preceding two comparisons extended from loading method 1 and 2, including the model simplification for loading method 2. They compared the relative displacement (circumferential) and torsional angle (circumferential) of the steel rings at both ends of the flexible pipe, calculated through both analytical derivation and simulation. Following the comparison of the two methods across all three scenarios, a certain degree of deviation was found, ranging from 2.43% to 4.18%. This range of deviation is relatively small and may be attributed to differences in the structural stiffness and assumptions between the two calculation methods, leading to slight discrepancies in the final results.

In conclusion, after comparing the data with the analytical modeling analysis, it can be concluded that the finite element analysis data presented above is reasonably reliable.

References

[1] LIANG Shang-jun, YANG Ke, NIU Xiao-kang, et al. Research Progress on Structural Domain of Morphing Aircraft[J]. Aircraft Design, 2017, 37(6) : 1-5.

[2] Armando R Rodriguez. Morphing Aircraft Technology Survey[R]. AIAA Paper 2007-1258, 2007.

ISSN: 2414-1895 DOI: 10.6919/ICJE.202312_9(12).0068

[3] Jason Bowman,Brian Sanders,Bryan Cannon,et al. Development of Next Generation Morphing Aircraft Structures[R]. AIAA Paper 2007-1730, 2007.

[4] Thomas G Ivanco,Robert C Scott,,Michael H Love, et al. Validation of the Lockheed Martin Morphing Concept with Wind Tunnel Testing[R]. AIAA Paper 2007-2235, 2007.

[5] Perry I, Boyd, Cole SR, Miller GD. Summary of an active flexible wing program. Journal of Aircraft. 1995; 32(1): 10-15.

[6] Garcia H, Abdulrahim M, Lind R. Roll control for a micro air vehicle using active wing morphing. Proc of the AIAA Guidance, Navigation, and Control Conference and Exhibit, Austin, Texas, 2003.

[7] Kudva JN, Sanders BP, Pinkerton-Florance JL, Garcia E. Overview of the DARPA/AFRL/NASA smart wing phase II program. Proc of the SPIE's 8th Annual International Symposium on Smart Structures and Materials, 2001.

[8] Kudva J. Overview of the DARPA smart wing project. Journal of intelligent material systems and structures. 2004;15(4):261-267.

[9] Florance JP, Burner AW, Fleming GA, Hunter CA, Graves SS, Martin CA. Contributions of the NASA Langley Research Center to the DARPA/AFRL/NASA/Northrop Grumman smart wing program. Technical Report, Norfolk, Virginia; 2003.

[10] Bartley-Cho JD, Wang DP, Martin CA, Kudva JN, West MN. Development of high-rate, adaptive trailing edge control surface for the smart wing phase 2 wind tunnel model. Journal of intelligent material systems and structures. 2004;15(4):279-291.

[11] Li Zhe, Ge Wenjie, Wang Heping, Topology Optimization Design of Shape Changing Compliant Mechanism for Wing Trailing Edge[J]. Computer simulation, 2009(03): 62-65.

[12] Zhu Penggang, Ge Wenjie, Zhang Yonghong, Zhao fei, Topology Optimization for Shape Morphing Compliant Trailing Edge Using SIMP and GA, Mechanical science and technology, 2009(11): 1468-1472.

[13] Zhang Long, Wang Heping, Ge Wenjie, Zhao Fei, A Compliant Rib Based Morphing Wing Geometric Parameters Design[J]. Aeronautical computing technology, 2009(01): 1-5.

[14] Jing Li, Zhang Yonghong, Ge Wenjie, Long Yongcheng, Topology Optimization for Shape Morphing Compliant Trailing Edge Using Multi-objective Load Path Approach[J], Mechanical Science and Technology for Aerospace Engineering, 2010(10): 1420-1425.

[15] Zhaofei, Ge Wenjie, Zhang Long, Topological optimization on the deformation mechanism of Flexible trailing edge of certain pilot-less aircraft, Journal of Machine Design. 2009(08): 19-22.